

Cite this: *Chem. Sci.*, 2022, 13, 3582

All publication charges for this article have been paid for by the Royal Society of Chemistry

## Chiral proline-substituted porous organic cages in asymmetric organocatalysis†

Ning Xu,<sup>a</sup> Kongzhao Su,<sup>ab</sup> El-Sayed M. El-Sayed,<sup>abd</sup> Zhanfeng Ju<sup>a</sup> and Daqiang Yuan<sup>ab\*</sup>

The efficient preparation of chiral porous organic cages (POCs) with specific functions is challenging, and their application in asymmetric catalysis has not previously been explored. In this work, we have achieved the construction of chiral POCs based on a supramolecular tetraformyl-resorcin[4]arene scaffold with different chiral proline-modified diamine ligands and utilizing dynamic imine chemistry. The incorporation of V-shaped or linear chiral diamines affords the [4 + 8] square prism and [6 + 12] octahedral POCs respectively. The appended chiral proline moieties in such POCs make them highly active supramolecular nanoreactors for asymmetric aldol reactions, delivering up to 92% ee. The spatial distribution of chiral catalytic sites in these two types of POCs greatly affects their catalytic activities and enantioselectivities. This work not only lays a foundation for the asymmetric catalytic application of chiral POCs, but also contributes to our understanding of the catalytic function of biomimetic supramolecular systems.

Received 21st January 2022

Accepted 3rd March 2022

DOI: 10.1039/d2sc00395c

rsc.li/chemical-science

## Introduction

Due to the importance of chiral molecules in the biomedical and environmental fields, acquiring high chiral purity compounds through asymmetric catalysis is a long-term pursuit of chemists.<sup>1</sup> In the recent decades, asymmetric organocatalysis has attracted considerable attention because of its avoidance of expensive or toxic metals and their pollution of catalytic products.<sup>2–4</sup> Immobilization of chiral functionalities on porous materials could realize enantioselective catalysis based on chiral porous materials.<sup>5–8</sup> To date, many solid porous materials, including metal–organic frameworks,<sup>9</sup> covalent organic frameworks<sup>10</sup> and porous organic polymers<sup>11</sup> have been widely employed as versatile platforms for asymmetric organocatalysis. The heterogeneous nature of extended frameworks leads to limited contact between the catalytically active sites and the substrates, and thus these chiral porous materials usually exhibit lower activity and stereoselectivity.<sup>12–15</sup> In contrast,

soluble porous materials may be more suitable candidates with which to achieve high-efficiency asymmetric catalysis.

Porous organic cages (POC),<sup>16–25</sup> which are assembled by individual organic molecules with guest-accessible intrinsic cavities, have shown vigorous development trends in many fields, such as gas storage and separation,<sup>26–32</sup> sensing,<sup>33–36</sup> host–guest chemistry,<sup>37–41</sup> and catalyst supports.<sup>42–47</sup> Compared with extended porous frameworks, POCs have clear advantages in solution processing, regeneration and functionalization.<sup>48,49</sup> Although the encapsulation of precious metal nanoparticles by the well-defined cavities of POCs can give rise to high catalytic activity, this will inevitably bring about a series of disadvantages characteristic of metal catalysis. Recently, the groups of Tiefenbacher and Neri have utilized a hexameric resorcinarene capsule to perform a variety of organic transformations inside the electron-rich aromatic cavity.<sup>50–52</sup> But the self-assembled capsule usually serves as a supramolecular host and requires the introduction of additional organic catalysts.<sup>53–56</sup> The rational integration of building blocks with embedded functional moieties offers a feasible solution for realizing metal-free catalysis based on POCs.<sup>57–59</sup> Theoretically, chiral POCs with asymmetric catalytic functions could also be constructed using a bottom-up synthetic strategy. Reasonable grafting of chiral active sites on cage skeletons or in cavities may create a catalytic environment similar to that in natural enzymes. However, the direct construction of chiral POCs with asymmetric catalytic functions remains challenging because the presence of chiral species can affect the crystallinity and self-assembly processes of POCs.<sup>60–64</sup> To date, utilization of chiral building units to

<sup>a</sup>State Key Laboratory of Structural Chemistry, Fujian Institute of Research on the Structure of Matter, Chinese Academy of Sciences, Fuzhou, 350002, Fujian, China. E-mail: ydq@fjirsm.ac.cn

<sup>b</sup>University of the Chinese Academy of Sciences, Beijing, 100049, China

<sup>c</sup>Fujian Science and Technology Innovation Laboratory for Optoelectronic Information of China, Fuzhou, 350002, Fujian, China

<sup>d</sup>Chemical Refining Laboratory, Refining Department, Egyptian Petroleum Research Institute, Nasr City, 11727, Egypt

† Electronic supplementary information (ESI) available. CCDC 2113144 and 2113665. For ESI and crystallographic data in CIF or other electronic format see DOI: 10.1039/d2sc00395c

construct chiral POCs for asymmetric catalysis remains unexploited.

As representative organocatalysts, proline and its derivatives are enamine- or imine catalysts effective for various asymmetric organic transformations.<sup>65–67</sup> The precise introduction of chiral proline moieties can endow POCs with outstanding enantioselective catalytic performance. We recently reported a series of POCs constructed from the tetraformyl-functionalized calix[4]-resorcinarene (C4RACHO) and different diamine linkers.<sup>68–70</sup> The diverse self-assembly forms and tunable window size and environment provide a promising platform for the chiral functionalization of calix[4]resorcinarene-based POCs.

Herein, we describe the design and synthesis of two chiral proline-decorated diamine ligands with different shapes and have employed them to react with C4RACHO to fabricate two homochiral POCs, CPOC-401-Pro and CPOC-302-Pro. These two chiral POCs feature distinct self-assembly behaviors and structural characteristics. The anchored chiral proline moieties enable them to efficiently catalyze asymmetric aldol reactions, an important C–C bond formation reaction in organic chemistry. Remarkably, the inherent chiral confined cavities cause the two cages to exhibit significantly improved catalytic activities over the model catalyst and *L*-proline. The different chiral catalytic selectivities of the cage catalysts demonstrate the importance of the spatial arrangement of organocatalytic sites in asymmetric catalysis based on chiral POCs. This study describes the great application potentials of chiral POCs in asymmetric catalysis, and could pave the way for development of highly efficient porous supramolecular organocatalysts.

## Results and discussion

### Design and synthesis of chiral proline-functionalized POCs

In order to construct chiral-functionalized POCs, we designed a general approach to introduce chiral proline units into the structure of diamine ligands through multi-step reactions. First, the *N*-Boc-*L*-proline moiety was incorporated into the precursor molecular structures through an amide coupling reaction. After removing the protecting group (Boc) at room temperature, the chiral proline-functionalized dinitro compounds (**A2** and **B2**) were easily obtained (see ESI† for details). Finally, through a mild reduction reaction, the chiral proline-decorated enantiopure diamine ligands (*S*)-*N*-(3,5-diaminophenyl)pyrrolidine-2-carboxamide (**A3**) and (*S*)-*N*-(4,4'-diamino-[1,1'-biphenyl]-2-yl)pyrrolidine-2-carboxamide (**B3**) were produced in high yields. The diamine ligands **A3** and **B3** could be regarded as the functionalized derivatives of the V-shaped *m*-phenylenediamine and linear 4,4'-diaminobiphenyl. Our previous work showed that the V-shaped phenylene-diamine linkers give rise to [3 + 6] trimeric triangular prisms, while the linear phenylene-diamine linkers lead to the formation of [6 + 12] hexameric octahedra. Because of the steric hindrance of the proline unit, the existence of chiral proline moieties in the linkers can not only affect the pore size and environment of POCs, but may also induce the formation of novel self-assembly forms.

To explore the influence of the chiral proline units on the self-assembly behaviors of calix[4]resorcinarene-based POCs, we first examined the self-assembly mode of the V-shaped diamine ligand (**A3**). Surprisingly, the reaction between C4RACHO and **A3** in CHCl<sub>3</sub> produced an unprecedented chiral [4 + 8] tetrameric cage CPOC-401-Pro (Fig. 1). Compared with the [3 + 6] trimeric triangular prisms, the [4 + 8] tetrameric square prism that was obtained has a larger window diameter, which undoubtedly weakens the steric hindrance caused by the bulky chiral proline groups. Although the isotopic distribution patterns of [3 + 6] trimeric cage were detected in reaction solutions, the crystalline samples of [4 + 8] tetrameric cage obtained by diffusion proved to be the main product. The good solubility of CPOC-401-Pro in common organic solvents facilitates its characterization in solution. Due to the keto-enamine tautomerization of the imine bonds in CPOC-401-Pro, two enamine-derived proton signals are observed at 9.27 and 16.05 ppm in the <sup>1</sup>H nuclear magnetic resonance (NMR) spectrum (Fig. S3†). Meanwhile, the amide proton signals are seen at 10.01 ppm, while the proton signals for pyrrolidine units are in the range of 1.74–3.82 ppm, suggesting the successful incorporation of chiral proline units. The structure of CPOC-401-Pro was further confirmed by 2D <sup>1</sup>H-<sup>1</sup>H COSY and <sup>1</sup>H DOSY tests (Fig. S4 and S5†). According to the DOSY spectrum, the diffusion coefficient (*D*) of CPOC-401-Pro is calculated to be 3.39 × 10<sup>−10</sup> m<sup>2</sup> s<sup>−1</sup> and the hydrodynamic radius calculated by the Stokes–Einstein equation is 1.13 nm. In the high-resolution electrospray ionization mass spectrometry (ESI-TOF-MS) of CPOC-401-Pro, the observed ion peak at *m/z* of 955.6886 corresponds to the [M + 5H]<sup>5+</sup> ion, unambiguously indicating the formation of [4 + 8] tetrameric cage (calculated *m/z* = 955.6889) (Fig. 2a). In addition, the chiral nature of CPOC-401-Pro was confirmed by its circular dichroism (CD) spectrum. As depicted in Fig. S16† in the ESI, the *L*-proline-substituted CPOC-401-Pro

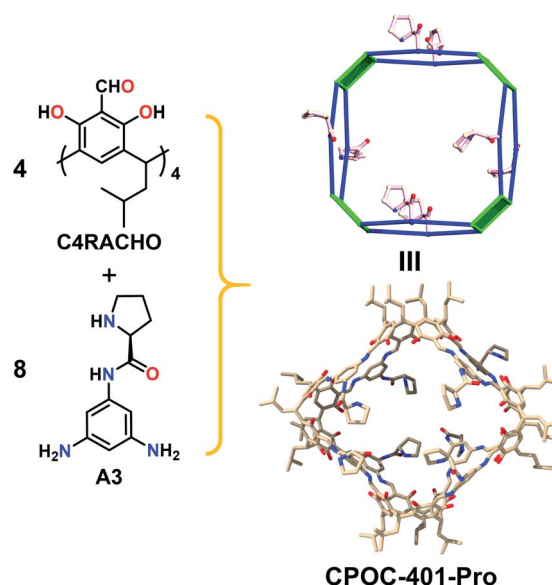


Fig. 1 The synthesis and structure of chiral [4 + 8] tetrameric cage CPOC-401-Pro. Hydrogen atoms are omitted for clarity.



Fig. 2 Experimental ESI-TOF-MS of CPOC-401-Pro (a), CPOC-302-Pro (b), and their simulated mass spectra.

and the D-proline-substituted CPOC-401-Pro display clear mirror image signals, thus demonstrating their opposite chirality.

Consistent with the previously reported self-assembly mode, the reaction of the linear diamine ligand (**B3**) with C4RACHO led smoothly to formation of the chiral hexameric octahedral cage CPOC-302-Pro (Fig. 3). The  $^1\text{H}$  NMR spectrum of CPOC-302-Pro shows the characteristic proton signals of proline units and the presence of keto-enamine tautomerization (Fig. S6†). The formation of the octahedral cage was further confirmed by 2D  $^1\text{H}$ - $^1\text{H}$  COSY and  $^1\text{H}$  DOSY spectra (Fig. S7 and S8†). The hydrodynamic radius of CPOC-302-Pro is calculated as 2.42 nm according to Stokes–Einstein equation. The ESI-TOF-MS spectrum of CPOC-302-Pro exhibits the  $[\text{M} + 5\text{H}]^{5+}$ ,  $[\text{M} + 6\text{H}]^{6+}$ , and  $[\text{M} + 7\text{H}]^{7+}$  ions at  $m/z$  of 1615.6061, 1346.5064 and 1154.2905, respectively, which are in accordance with the theoretically calculated values (Fig. 2b and S12–S14†). The optical activity of CPOC-302-Pro was also confirmed by its CD spectrum, as shown in Fig. S17.†

### X-ray crystal structures of CPOC-401-Pro and CPOC-302-Pro

Single-crystal X-ray diffraction analysis shows that CPOC-401-Pro crystallizes in a triclinic system with the space group  $P1$ . Due to the very weak and low-resolution diffraction data, the

accurate atomic positions of the substituents in CPOC-401-Pro cannot be located and refined, but two complete molecular cage units were observed in each asymmetric unit through the electron-density map. The cage with substituents was modeled *in silico* and optimized the GFN1-xTB method with Grimme's D3 van der Waals dispersion correction using the CP2K code based on the preliminary crystal data. The results of both the experiment and the simulation showed that each cage molecule is constructed with four C4RACHO as the vertices, and eight **A3** molecules as the edges, thus forming a tetrameric prism structure with eight chiral proline groups modified on the cage skeleton (Fig. 1). Compared with the  $[3 + 6]$  trimeric triangular prisms, the  $[4 + 8]$  tetrameric square prisms that were obtained should be self-assembly forms with relatively lower energy because of the bulky chiral proline moieties. This result suggests that the presence of substituents may lead to changes in the self-assembly mode of POCs.

Structural analysis of CPOC-302-Pro reveals that it crystallizes in a trigonal system with the space group  $P3c1$ . It also shows two cage molecules per unit cell and its structure is similar to that of the previously reported CPOC-302, which features a large octahedral cage and eight trigonal windows (Fig. 3). Due to the various forms of **B3** molecules in the self-assembly process, the structure of CPOC-302-Pro contains multiple isomers, and the anchored L-proline units could not be assigned a fixed position from the diffraction data due to severe disorder. However, the octahedral structure of CPOC-302-Pro could be confirmed from its single-crystal data.

### Permanent porosity of CPOC-401-Pro and CPOC-302-Pro

The porosity of the synthesized chiral POCs was examined by  $\text{N}_2$  sorption experiments on the activated samples at 77 K. As shown in Fig. 4, the adsorption isotherms of CPOC-401-Pro and CPOC-302-Pro exhibit a combination of type I and type IV, which indicates highly porous structures. Their Brunauer–Emmett–Teller (BET) surface areas were calculated to be 648 and  $861 \text{ m}^2 \text{ g}^{-1}$ , respectively, and the calculated micropore



Fig. 3 The synthesis and structure of chiral  $[6 + 12]$  hexameric cage CPOC-302-Pro. Hydrogen atoms have been omitted for clarity.

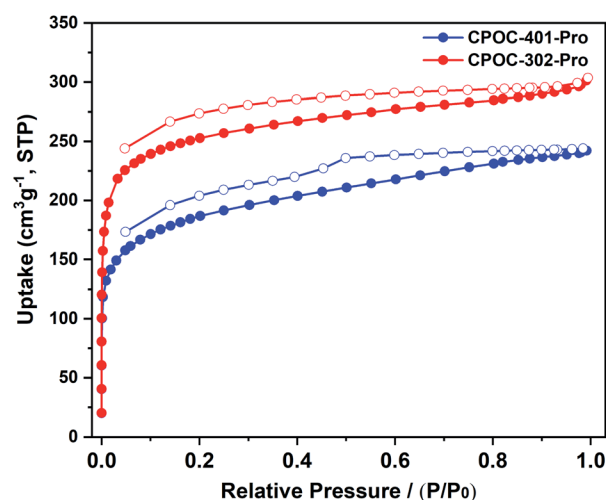


Fig. 4  $\text{N}_2$  sorption isotherms of CPOC-401-Pro and CPOC-302-Pro at 77 K.



volumes were 0.14 and 0.26 cm<sup>3</sup> g<sup>-1</sup>. The N<sub>2</sub> sorption capacity and the BET value of CPOC-302-Pro are significantly reduced relative to the unsubstituted assembly structure (CPOC-302), and this is attributed to the channels blocking the proline units. The permanent porosity of the two chiral POCs would promote the effective contact between catalytic centers and the substrates, and accelerate the reaction within the cavities.

### Asymmetric organocatalysis

Because of the tolerant reaction conditions and the avoidance of toxic metals,<sup>71</sup> asymmetric organocatalysis represents an environmentally benign catalytic methodology in asymmetric synthesis. Asymmetric aldol addition is a typical atom-economic reaction producing enantiomerically enriched  $\beta$ -hydroxy ketones, an important structural motif in many natural and biologically active compounds.<sup>72</sup> It is commonly acknowledged that proline and its derivatives are the most privileged organocatalysts for aldol reactions, and they have been extensively immobilized on diverse supports for use as heterogeneous catalysts. However, these catalysts in general exhibit low activities and unsatisfactory stereoselectivities as a result of the low accessibility of the catalytic sites. By virtue of the unique solution processability and inherent internal voids, POCs could be regarded as ideal platforms for the design of highly active catalytic materials as they can easily realize the efficient access to catalytic centers and the transport of reactants and products. The fruitful chiral proline units endow CPOC-401-Pro and CPOC-302-Pro with the enzyme-mimicking chiral cavity micro-environments which could facilitate the asymmetric aldol reaction.

The aldol addition of *p*-nitrobenzaldehyde with cyclohexanone was selected as a model reaction with which to assess the catalytic activity of the two chiral POCs. As shown in Table 1, with 10 mol% loadings of effective chiral proline groups in CPOC-401-Pro and CPOC-302-Pro, the aldol reaction proceeded cleanly and smoothly with 100% conversion. Among these,

CPOC-302-Pro effectively promotes the reaction, affording the desired product in 99% yield with ee and dr values of 92% and 93 : 7, respectively. In contrast, CPOC-401-Pro gave relatively low ee and dr values despite the faster reaction rate (entries 1 and 2). The kinetic study of the model reaction revealed that CPOC-302-Pro did give rise to higher enantioselectivity, but the reaction rate was lower (Fig. S21†). Considering that CPOC-401-Pro and CPOC-302-Pro possess the same chiral catalytic sites, the above results show that the difference in the spatial distribution of chiral organocatalytic sites caused by the distinct characteristics of the self-assembly forms of chiral POCs could have a significant impact on the catalytic performance.

For comparison, a model catalyst, BPP with the same catalytic structure as CPOC-302-Pro was prepared to catalyze the asymmetric aldol addition under otherwise identical conditions. It can be seen in Table 1 that BPP required an appreciably longer reaction time than CPOC-302-Pro (entry 3). The enhanced catalytic activity of CPOC-302-Pro may be due to the accumulation of reactants in the cavity and the more efficient contact between active sites and the substrates in the chiral and confined space. Meanwhile, slightly lower enantioselectivity and diastereoselectivity were observed when the model catalyst BPP was used. The catalytic property of L-proline under the same conditions was also evaluated. Compared to the two chiral POCs, L-proline was extremely inert catalytically, and required 10 days to complete the reaction, which had significantly lower diastereoselectivity and diminished enantioselectivity (entry 4). Although a variety of proline-functionalized porous/supramolecular materials have been used to catalyze the asymmetric aldol reaction, these materials gave unsatisfactory enantioselectivity and/or diastereoselectivity.<sup>13,15,73–79</sup> In comparison, the chiral POC-based supramolecular catalyst CPOC-302-Pro exhibited much superior catalytic performance (Table S2†). The D-proline-decorated CPOC-401-Pro and CPOC-302-Pro displayed opposite chiral induction effects, suggesting the powerful chiral confinement abilities of the two chiral POCs, which could expediently regulate the product enantioselectivity (entries 5 and 6).

Subsequently to illustrate the generality of the chiral POC catalysts, we investigated the scope of substrates. The products that were obtained catalyzed by CPOC-302-Pro are presented in Table 2. It was found that aromatic aldehydes substituted with various electron-withdrawing groups such as nitro, cyano, trifluoromethyl and pyridine can be employed with cyclohexanone leading to the corresponding products with excellent yields (90–99%) and stereoselectivities (80 : 20–97 : 3 dr values, 87–92% ee values). Substituted cyclohexanones and tetrahydropyran-4-one were also found to be well-tolerated, affording the desired products in high yields with good stereoselectivity. In order to acquire higher enantioselectivity, the reactions of substrates, including cyclopentanone and acetone, with smaller molecular volume, were studied at 0 °C. It was observed that cyclopentanone could react with *p*-nitrobenzaldehyde to provide the product with good enantioselectivity (86% ee), while the reaction between acetone and *p*-nitrobenzaldehyde affords only moderate enantioselectivity (64% ee). CPOC-401-Pro can also efficiently catalyze this series of reactions, but the afforded

**Table 1** Asymmetric aldol reactions catalyzed by chiral POCs and related catalysts<sup>a</sup>



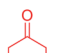
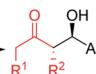
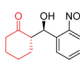
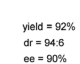
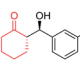
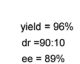
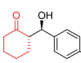
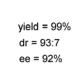
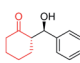
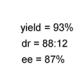
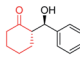
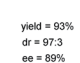
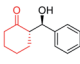
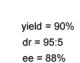
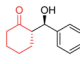
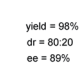
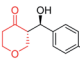
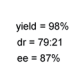
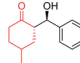
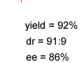
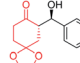
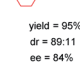
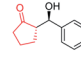
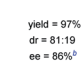
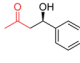
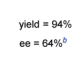
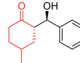
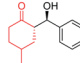
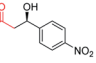
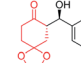
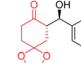
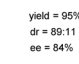
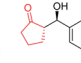
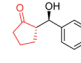
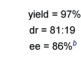
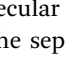
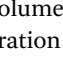
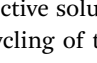
Entry <sup>a</sup>	Catalyst	Time (d)	Yield <sup>b</sup> (%)	anti/syn <sup>c</sup>	ee <sup>d</sup> (%)
1	CPOC-401-Pro	1	98	88 : 12	83
2	CPOC-302-Pro	2	99	93 : 7	92
3	BPP	4	96	89 : 11	88
4	L-Proline	10	80	45 : 55	77
5 <sup>e</sup>	CPOC-401-Pro	1	97	88 : 12	–83
6 <sup>f</sup>	CPOC-302-Pro	2	98	93 : 7	–91

<sup>a</sup> Reaction conditions: aldehyde (0.20 mmol), ketone (2.0 mmol), 10 mol% catalyst (related to the quantity of proline in the material), 4-nitrobenzoic acid (4-NBA) (20 mol%), H<sub>2</sub>O (0.01 mL), and MTBE (1.0 mL). <sup>b</sup> Isolated yield. <sup>c</sup> Determined by <sup>1</sup>H NMR. <sup>d</sup> Determined by chiral HPLC. <sup>e</sup> Catalyzed by D-proline-substituted CPOC-401-Pro. <sup>f</sup> Catalyzed by D-proline-substituted CPOC-302-Pro.





**Table 2** Substrate scope of the aldol addition reactions catalyzed by CPOC-302-Pro<sup>a</sup>

ArCHO + 		CPOC-302-Pro, 4-NBA (20 mol%) MTBE/H <sub>2</sub> O=100/1, r.t.			
					yield = 92% dr = 94:6 ee = 90%
					yield = 96% dr = 90:10 ee = 89%
					yield = 99% dr = 93:7 ee = 92%
					yield = 93% dr = 88:12 ee = 87%
					yield = 93% dr = 97:3 ee = 89%
					yield = 90% dr = 95:5 ee = 88%
					yield = 98% dr = 80:20 ee = 89%
					yield = 98% dr = 79:21 ee = 87%
					yield = 92% dr = 91:9 ee = 86%
					yield = 95% dr = 89:11 ee = 84%
					yield = 97% dr = 81:19 ee = 86% <sup>b</sup>
					yield = 94% ee = 84% <sup>b</sup>

<sup>a</sup> Reaction conditions: aldehyde (0.20 mmol), ketone (2.0 mmol), 10 mol% catalyst (relative to the quantity of proline in the material), 4-NBA (20 mol%), H<sub>2</sub>O (0.01 mL), and MTBE (1.0 mL) at r.t. for 3 days. Isolated yield. The above catalytic products were characterized by <sup>1</sup>H NMR and their ee values were determined by chiral HPLC.

<sup>b</sup> Under the 0 °C reaction conditions.

enantioselectivities and diastereoselectivities are lower than those from CPOC-302-Pro (Table S3†). This result further highlights the significant influence of the spatial arrangement of chiral sites on the catalytic processes of chiral POCs.

To probe the role of the cage cavity in catalysis processes, the 2D NOESY NMR studies of the mixture of CPOC-302-Pro and the reactants including *p*-nitrobenzaldehyde and cyclohexanone were performed (see ESI†). The NOESY NMR spectra clearly show that both *p*-nitrobenzaldehyde and cyclohexanone could be encapsulated inside the cavity of CPOC-302-Pro. Furthermore, a size selectivity study was conducted (see ESI†). First, we designed 5-formyl-2-nitrophenyl-3,5-di-*tert*-butylbenzoate, an aldehyde

substrate with a large diameter ( $8.88 \times 10.81 \text{ \AA}^2$ ). The reaction between the bulky aldehyde and cyclohexanone in the presence of the model catalyst BPP gave a conversion of 85% after two days. In contrast, the efficiency for the aldol reaction catalyzed by CPOC-302-Pro was greatly decreased, and the conversion was only 35% after the same reaction time. The small window diameter (9.3 Å) of the unsubstituted assembly structure of CPOC-302-Pro, together with the hindrance offered by the proline units on the cage skeleton will prevent the bulky substrate binding in the cavity and lead to the aldol addition occurring mainly on the external surface of the cage. The above experiments provide convincing evidence that the majority of the catalytic reaction did take place inside the cavity of CPOC-302-Pro.

The repeated use of catalysts is important for sustainable applications. Typically, recovery and recycling of small-molecule organocatalysts is quite difficult. In contrast, however, the large molecular volume and selective solubility of POCs could facilitate the separation and recycling of the cage catalysts. Upon completion of the catalytic reaction, CPOC-302-Pro can be easily recovered as a precipitate which is produced by adding *n*-hexane into the reaction solution and which should be washed several times with *n*-hexane prior to its next use. The test results indicated that CPOC-302-Pro retained its activity, enantio-selectivity and diastereoselectivity after five cycles, as illustrated in Fig. 5. ESI-TOF-MS (Fig. S15†) showed that the recovered samples of CPOC-302-Pro retained the original structure. The robustness of the cage catalyst greatly benefits its practical applications. Combining all of the catalytic features described above, CPOC-302-Pro could function as a high-performance homogeneous asymmetric catalyst with prominent enantioselective catalytic activity, broad substrate scope and good recyclability.

## Conclusions

In summary, we have developed the first example of a chiral POC for asymmetric catalysis using a bottom-up synthetic strategy. Two calix[4]resorcinarene-based chiral POCs (tetrameric prismatic CPOC-401-Pro and hexameric octahedral CPOC-302-Pro) were successfully constructed by the self-assembly of the 4-connected C4RACHO cavitand and chiral proline-substituted diamine ligands with different shapes. The inherent confined cavities and the abundant chiral proline catalytic centers allow the two chiral POCs to serve as efficient metal-free supramolecular catalysts for the asymmetric aldol reaction with significantly boosted enantioselective catalytic performance. Through comparison, we found that the spatial distribution of chiral catalytic sites in CPOC-401-Pro and CPOC-302-Pro plays an important role in their catalytic processes. Considering that a substantial number of chiral catalytic groups can be reasonably attached to the structure of POCs, it is anticipated that this work will initiate the exploration of various asymmetric catalytic processes based on chiral POCs.

## Data availability

All the data have been included in the ESI.†



Fig. 5 Recycling tests of CPOC-302-Pro for asymmetric aldol reactions.



## Author contributions

D. Yuan conceived the research project. N. Xu performed the experiments and the data analyses. All authors contributed to the analysis and writing.

## Conflicts of interest

There are no conflicts to declare.

## Acknowledgements

The authors thank the support of the National Natural Science Foundation of China (22071244 and 21905281), China Postdoctoral Science Foundation (2020M671954), the Key Research Program of Frontier Sciences, Chinese Academy of Sciences (QYZDB-SSW-SLH019), and the Natural Science Foundation of Fujian Province (2017J01032).

## Notes and references

- 1 D. P. Glavin, A. S. Burton, J. E. Elsil, J. C. Aponte and J. P. Dworkin, *Chem. Rev.*, 2020, **120**, 4660–4689.
- 2 D. W. C. MacMillan, *Nature*, 2008, **455**, 304–308.
- 3 N. Wang, Z. Wu, J. Wang, N. Ullah and Y. Lu, *Chem. Soc. Rev.*, 2021, **50**, 9766–9793.
- 4 S.-H. Xiang and B. Tan, *Nat. Commun.*, 2020, **11**, 3786.
- 5 M. Yoon, R. Srirambalaji and K. Kim, *Chem. Rev.*, 2012, **112**, 1196–1231.
- 6 X. Han, C. Yuan, B. Hou, L. Liu, H. Li, Y. Liu and Y. Cui, *Chem. Soc. Rev.*, 2020, **49**, 6248–6272.
- 7 H. Zhang, L.-L. Lou, K. Yu and S. Liu, *Small*, 2021, **17**, 2005686.
- 8 T. Hong, Z. Zhang, Y. Sun, J.-J. Tao, J.-D. Tang, C. Xie, M. Wang, F. Chen, S.-S. Xie, S. Li and P. J. Stang, *J. Am. Chem. Soc.*, 2020, **142**, 10244–10249.
- 9 W. Gong, X. Chen, H. Jiang, D. Chu, Y. Cui and Y. Liu, *J. Am. Chem. Soc.*, 2019, **141**, 7498–7508.
- 10 H. Xu, J. Gao and D. Jiang, *Nat. Chem.*, 2015, **7**, 905–912.
- 11 Q. Sun, Z. Dai, X. Meng and F.-S. Xiao, *Chem. Mater.*, 2017, **29**, 5720–5726.
- 12 H. Xu, X. Chen, J. Gao, J. Lin, M. Addicoat, S. Irle and D. Jiang, *Chem. Commun.*, 2014, **50**, 1292–1294.
- 13 C. Kutzscher, G. Nickerl, I. Senkovska, V. Bon and S. Kaskel, *Chem. Mater.*, 2016, **28**, 2573–2580.
- 14 Y. Lan, C. Yang, Y. Zhang, W. An, H. Xue, S. Ding, P. Zhou and W. Wang, *Polym. Chem.*, 2019, **10**, 3298–3305.
- 15 P. Chen, J.-S. Sun, L. Zhang, W.-Y. Ma, F. Sun and G. Zhu, *Sci. China Mater.*, 2019, **62**, 194–202.
- 16 T. Hasell and A. I. Cooper, *Nat. Rev. Mater.*, 2016, **1**, 16053.
- 17 M. Mastalerz, *Acc. Chem. Res.*, 2018, **51**, 2411–2422.
- 18 G. Zhang and M. Mastalerz, *Chem. Soc. Rev.*, 2014, **43**, 1934–1947.
- 19 A. G. Slater, M. A. Little, A. Pulido, S. Y. Chong, D. Holden, L. Chen, C. Morgan, X. Wu, G. Cheng, R. Clowes, M. E. Briggs, T. Hasell, K. E. Jelfs, G. M. Day and A. I. Cooper, *Nat. Chem.*, 2017, **9**, 17–25.
- 20 F. Beuerle and B. Gole, *Angew. Chem., Int. Ed.*, 2018, **57**, 4850–4878.
- 21 K. Acharyya and P. S. Mukherjee, *Angew. Chem., Int. Ed.*, 2019, **58**, 8640–8653.
- 22 S. Bera, A. Basu, S. Tothadi, B. Garai, S. Banerjee, K. Vanka and R. Banerjee, *Angew. Chem., Int. Ed.*, 2017, **56**, 2123–2126.
- 23 S. Ivanova, E. Köster, J. J. Holstein, N. Keller, G. H. Clever, T. Bein and F. Beuerle, *Angew. Chem., Int. Ed.*, 2021, **60**, 17455–17463.
- 24 S. Hong, M. R. Rohman, J. Jia, Y. Kim, D. Moon, Y. Kim, Y. H. Ko, E. Lee and K. Kim, *Angew. Chem., Int. Ed.*, 2015, **54**, 13241–13244.
- 25 Z. Sun, P. Li, S. Xu, Z.-Y. Li, Y. Nomura, Z. Li, X. Liu and S. Zhang, *J. Am. Chem. Soc.*, 2020, **142**, 10833–10840.
- 26 M. Liu, L. Zhang, M. A. Little, V. Kapil, M. Ceriotti, S. Yang, L. Ding, D. L. Holden, R. Balderas-Xicohtencatl, D. He, R. Clowes, S. Y. Chong, G. Schütz, L. Chen, M. Hirscher and A. I. Cooper, *Science*, 2019, **366**, 613–620.
- 27 Z. Wang, N. Sikdar, S.-Q. Wang, X. Li, M. Yu, X.-H. Bu, Z. Chang, X. Zou, Y. Chen, P. Cheng, K. Yu, M. J. Zaworotko and Z. Zhang, *J. Am. Chem. Soc.*, 2019, **141**, 9408–9414.
- 28 T. Hasell, M. Miklitz, A. Stephenson, M. A. Little, S. Y. Chong, R. Clowes, L. Chen, D. Holden, G. A. Tribello, K. E. Jelfs and A. I. Cooper, *J. Am. Chem. Soc.*, 2016, **138**, 1653–1659.
- 29 L. Chen, P. S. Reiss, S. Y. Chong, D. Holden, K. E. Jelfs, T. Hasell, M. A. Little, A. Kewley, M. E. Briggs, A. Stephenson, K. M. Thomas, J. A. Armstrong, J. Bell, J. Busto, R. Noel, J. Liu, D. M. Strachan, P. K. Thallapally and A. I. Cooper, *Nat. Mater.*, 2014, **13**, 954–960.
- 30 A. S. Bhat, S. M. Elbert, W.-S. Zhang, F. Rominger, M. Dieckmann, R. R. Schröder and M. Mastalerz, *Angew. Chem., Int. Ed.*, 2019, **58**, 8819–8823.
- 31 Y. Ding, L. O. Alimi, B. Moosa, C. Maaliki, J. Jacquemin, F. Huang and N. M. Khashab, *Chem. Sci.*, 2021, **12**, 5315–5318.
- 32 B. Moosa, L. O. Alimi, A. Shkurenko, A. Fakim, P. M. Bhatt, G. Zhang, M. Eddaoudi and N. M. Khashab, *Angew. Chem., Int. Ed.*, 2020, **59**, 21367–21371.
- 33 X. Zheng, W. Zhu, C. Zhang, Y. Zhang, C. Zhong, H. Li, G. Xie, X. Wang and C. Yang, *J. Am. Chem. Soc.*, 2019, **141**, 4704–4710.
- 34 M. Brutschy, M. W. Schneider, M. Mastalerz and S. R. Waldvogel, *Adv. Mater.*, 2012, **24**, 6049–6052.
- 35 T. Jiao, L. Chen, D. Yang, X. Li, G. Wu, P. Zeng, A. Zhou, Q. Yin, Y. Pan, B. Wu, X. Hong, X. Kong, V. M. Lynch, J. L. Sessler and H. Li, *Angew. Chem., Int. Ed.*, 2017, **56**, 14545–14550.
- 36 P. E. Alexandre, W. S. Zhang, F. Rominger, S. M. Elbert, R. R. Schroder and M. Mastalerz, *Angew. Chem., Int. Ed.*, 2020, **59**, 19675–19679.
- 37 M. Ortiz, S. Cho, J. Niklas, S. Kim, O. G. Poluektov, W. Zhang, G. Rumbles and J. Park, *J. Am. Chem. Soc.*, 2017, **139**, 4286–4289.
- 38 H. Duan, Y. Li, Q. Li, P. Wang, X. Liu, L. Cheng, Y. Yu and L. Cao, *Angew. Chem., Int. Ed.*, 2020, **59**, 10101–10110.



- 39 C. Zhang, Q. Wang, H. Long and W. Zhang, *J. Am. Chem. Soc.*, 2011, **133**, 20995–21001.
- 40 V. Leonhardt, S. Fimmel, A.-M. Krause and F. Beuerle, *Chem. Sci.*, 2020, **11**, 8409–8415.
- 41 H. Nian, L. Cheng, L. Wang, H. Zhang, P. Wang, Y. Li and L. Cao, *Angew. Chem., Int. Ed.*, 2021, **60**, 15354–15358.
- 42 N. Sun, C. Wang, H. Wang, L. Yang, P. Jin, W. Zhang and J. Jiang, *Angew. Chem., Int. Ed.*, 2019, **58**, 18011–18016.
- 43 X. Yang, J.-K. Sun, M. Kitta, H. Pang and Q. Xu, *Nat. Catal.*, 2018, **1**, 214–220.
- 44 B. Mondal and P. S. Mukherjee, *J. Am. Chem. Soc.*, 2018, **140**, 12592–12601.
- 45 L. Qiu, R. McCaffrey, Y. Jin, Y. Gong, Y. Hu, H. Sun, W. Park and W. Zhang, *Chem. Sci.*, 2018, **9**, 676–680.
- 46 S. Gao, Y. Liu, L. Wang, Z. Wang, P. Liu, J. Gao and Y. Jiang, *ACS Catal.*, 2021, **11**, 5544–5553.
- 47 S.-Y. Zhang, Z. Kochovski, H.-C. Lee, Y. Lu, H. Zhang, J. Zhang, J.-K. Sun and J. Yuan, *Chem. Sci.*, 2019, **10**, 1450–1456.
- 48 Q. Song, S. Jiang, T. Hasell, M. Liu, S. Sun, A. K. Cheetham, E. Sivaniah and A. I. Cooper, *Adv. Mater.*, 2016, **28**, 2629–2637.
- 49 N. Giri, M. G. Del Pópolo, G. Melaugh, R. L. Greenaway, K. Rätzke, T. Koschine, L. Pison, M. F. C. Gomes, A. I. Cooper and S. L. James, *Nature*, 2015, **527**, 216–220.
- 50 Q. Zhang and K. Tiefenbacher, *Nat. Chem.*, 2015, **7**, 197–202.
- 51 Q. Zhang, J. Rinkel, B. Goldfuss, J. S. Dickschat and K. Tiefenbacher, *Nat. Catal.*, 2018, **1**, 609–615.
- 52 P. La Manna, C. Talotta, G. Floresta, M. De Rosa, A. Soriente, A. Rescifina, C. Gaeta and P. Neri, *Angew. Chem., Int. Ed.*, 2018, **57**, 5423–5428.
- 53 P. La Manna, M. De Rosa, C. Talotta, A. Rescifina, G. Floresta, A. Soriente, C. Gaeta and P. Neri, *Angew. Chem., Int. Ed.*, 2020, **59**, 811–818.
- 54 T. M. Bräuer, Q. Zhang and K. Tiefenbacher, *Angew. Chem., Int. Ed.*, 2016, **55**, 7698–7701.
- 55 T. M. Bräuer, Q. Zhang and K. Tiefenbacher, *J. Am. Chem. Soc.*, 2017, **139**, 17500–17507.
- 56 P. La Manna, M. De Rosa, C. Talotta, C. Gaeta, A. Soriente, G. Floresta, A. Rescifina and P. Neri, *Org. Chem. Front.*, 2018, **5**, 827–837.
- 57 J. Koo, I. Kim, Y. Kim, D. Cho, I.-C. Hwang, R. D. Mukhopadhyay, H. Song, Y. H. Ko, A. Dhamija, H. Lee, W. Hwang, S. Kim, M.-H. Baik and K. Kim, *Chem.*, 2020, **6**, 3374–3384.
- 58 C. Liu, K. Liu, C. Wang, H. Liu, H. Wang, H. Su, X. Li, B. Chen and J. Jiang, *Nat. Commun.*, 2020, **11**, 1047.
- 59 X. Feng, P. Liao, J. Jiang, J. Shi, Z. Ke and J. Zhang, *ChemPhotoChem*, 2019, **3**, 1014–1019.
- 60 P. Wagner, F. Rominger, W. S. Zhang, J. H. Gross, S. M. Elbert, R. R. Schroder and M. Mastalerz, *Angew. Chem., Int. Ed.*, 2021, **60**, 8896–8904.
- 61 D. Beaudoin, F. Rominger and M. Mastalerz, *Angew. Chem., Int. Ed.*, 2017, **56**, 1244–1248.
- 62 E. Ramakrishna, J.-D. Tang, J.-J. Tao, Q. Fang, Z. Zhang, J. Huang and S. Li, *Chem. Commun.*, 2021, **57**, 9088–9091.
- 63 H. Qu, X. Tang, X. Wang, Z. Li, Z. Huang, H. Zhang, Z. Tian and X. Cao, *Chem. Sci.*, 2018, **9**, 8814–8818.
- 64 X. Tang, Z. Li, H. Liu, H. Qu, W. Gao, X. Dong, S. Zhang, X. Wang, A. C. H. Sue, L. Yang, K. Tan, Z. Tian and X. Cao, *Chem. Sci.*, 2021, **12**, 11730–11734.
- 65 B. List, *Acc. Chem. Res.*, 2004, **37**, 548–557.
- 66 F. An, B. Maji, E. Min, A. R. Ofial and H. Mayr, *J. Am. Chem. Soc.*, 2020, **142**, 1526–1547.
- 67 L.-W. Xu, L. Li and Z.-H. Shi, *Adv. Synth. Catal.*, 2010, **352**, 243–279.
- 68 K. Su, W. Wang, S. Du, C. Ji, M. Zhou and D. Yuan, *J. Am. Chem. Soc.*, 2020, **142**, 18060–18072.
- 69 W. Wang, K. Su, E.-S. M. El-Sayed, M. Yang and D. Yuan, *ACS Appl. Mater. Interfaces*, 2021, **13**, 24042–24050.
- 70 K. Su, W. Wang, S. Du, C. Ji and D. Yuan, *Nat. Commun.*, 2021, **12**, 3703.
- 71 B. List, *Chem. Rev.*, 2007, **107**, 5413–5415.
- 72 B. M. Trost and C. S. Brindle, *Chem. Soc. Rev.*, 2010, **39**, 1600–1632.
- 73 M. Banerjee, S. Das, M. Yoon, H. J. Choi, M. H. Hyun, S. M. Park, G. Seo and K. Kim, *J. Am. Chem. Soc.*, 2009, **131**, 7524–7525.
- 74 D. Dang, P. Wu, C. He, Z. Xie and C. Duan, *J. Am. Chem. Soc.*, 2010, **132**, 14321–14323.
- 75 D. J. Lun, G. I. N. Waterhouse and S. G. Telfer, *J. Am. Chem. Soc.*, 2011, **133**, 5806–5809.
- 76 Y. Liu, X. Xi, C. Ye, T. Gong, Z. Yang and Y. Cui, *Angew. Chem., Int. Ed.*, 2014, **53**, 13821–13825.
- 77 W.-L. He, M. Zhao and C.-D. Wu, *Angew. Chem., Int. Ed.*, 2019, **58**, 168–172.
- 78 J. Zhang, X. Han, X. Wu, Y. Liu and Y. Cui, *J. Am. Chem. Soc.*, 2017, **139**, 8277–8285.
- 79 X. Wu, C. He, X. Wu, S. Qu and C. Duan, *Chem. Commun.*, 2011, **47**, 8415–8417.

